An Adaptive Detector with Range Estimation Capabilities for Partially Homogeneous Environment

A. De Maio, *Fellow, IEEE*, C. Hao, *Member, IEEE*, and D. Orlando, *Senior Member, IEEE*

***Abstract*—In this work, we devise an adaptive decision scheme with range estimation capabilities for point-like targets in partially homogeneous environments. To this end, we exploit the spillover of target energy to consecutive range samples and synthesize the Generalized Likelihood Ratio Test. The performance analysis, conducted resorting to both simulated data and real recorded datasets, highlights that the newly proposed architecture can guarantee superior detection performance with respect to its competitors while retaining accurate estimation capabilities of the target position.**

***Index Terms*—Adaptive radar detection, constant false alarm rate (CFAR), generalized likelihood ratio test (GLRT), partially homogeneous environment, range estimation.**

I. Introduction

ADAPTIVE radar detection of point-like or extended targets embedded in Gaussian disturbance represents an active field of research, wherein the seminal paper by Kelly [1] and the technical report [2] are considered points of reference. Indeed, most recent papers rely on the results contained in the above works. Specifically, in [1], Kelly resorts to the Generalized Likelihood Ratio Test (GLRT) to derive a Constant False Alarm Rate (CFAR) test for detecting signals known up to a scaling factor. In [3], the authors derive another CFAR detector called Adaptive Matched Filter (AMF) using a two-step GLRT-based design procedure. Other different solutions can be found in open literature (see for instance [4]). All the above receivers assume a Homogeneous Environment (HE), wherein a set of secondary data free of signal components, but sharing the same spectral properties of the interference in the cells under test (primary data), is available. However, secondary data are often contaminated by power variations over range, clutter discretes, and other outliers, that could make secondary data not representative of the primary data. In such situations, receivers designed for the HE exhibit significant performance degradations and the CFAR property is no longer ensured [5]. A slightly general noise model assumes that the interference covariance matrix of the primary data and that of secondary data coincide only up to a scale factor. This scenario is referred to as Partially-Homogeneous Environment (PHE) and has been proposed in [6], where the authors apply the GLRT to get a fully-adaptive detector, referred to as the Adaptive Coherence Estimator (ACE) or the Adaptive Normalized Matched Filter (ANMF) [7].

Another important issue concerns the design assumptions of the nominal target. More precisely, detectors considered so far assume that the target is located exactly "where the matched filter is sampled" and, hence, that there is no straddle loss, namely no spillover of target energy to adjacent matched filter returns. While this is a reasonable approach, it does not fully use the information provided by the measurements from the two sampling points and, hence, does not share optimality properties [8]. In [8], it is assumed that several closely spaced targets fall within the same beam of a monopulse radar and among three or more adjacent matched filter samples in range; for the considered scenario a Maximum Likelihood (ML) extractor is developed that, using monopulse information from the above samples, estimates the angles and ranges of the targets. In [9], the authors focus on space-time adaptive processing [10], [11] and devise decision schemes for point-like targets which suitably exploit the spillover of target energy to provide accurate estimates of the target position within the cell under test (sub-bin accuracy). The range gates are formed sampling the output of a filter matched to the transmitted pulse, $p(t)$ say, every T_p seconds with T_p the duration of $p(t)$. At the design stage the authors assume either the HE or the PHE. Moreover, it is also shown that decision schemes conceived to detect distributed targets, see [2], [12]–[14], can be used to account for the spillover of a point-like target.

In the present work, we focus on the design of space-time decision schemes to detect point-like targets in PHE. More precisely, we borrow the discrete-time model of the received signal from [9] and apply the GLRT design criterion (it is important to stress here that in [9] the authors make use of the two-step GLRT design procedure in the case of PHE). The performance analysis is carried out on both simulated and real recorded data in comparison with the *ad hoc* detector derived in [9] for the PHE. Finally, it is important to highlight that the newly proposed architecture guarantees the CFAR property with respect to the unknown parameters of the disturbance.

The remainder of the paper is organized as follows. Next section is devoted to the problem formulation. Section III focuses on the detector design, while Section IV provides illustrative examples. Section V contains some concluding remarks and hints for future work.

II. Problem Formulation

The discrete-time model for the signal and the interference is borrowed from [9]. For the reader ease, we recall here that the

Manuscript received September 15, 2013; revised January 14, 2014; accepted January 17, 2014. Date of publication January 21, 2014; date of current version January 30, 2014. This work of was partially supported by the National Natural Science Foundation of China under Grants 61172166 and 61222107. The associate editor coordinating the review of this manuscript and approving it for publication was Prof. Joseph Tabrikian.

A. De Maio is with the Dipartimento di Ingegneria Elettrica e delle Tecnologie dell'Informazione, Università degli Studi di Napoli "Federico II," I-80125 Napoli, Italy (e-mail: ademaio@unina.it).

C. Hao is with the State Key Laboratory of Acoustics, Institute of Acoustics, Chinese Academy of Sciences, 100190 Beijing, China (e-mail: haochengp@mail.ioa.ac.cn).

D. Orlando is with ELETTRONICA S.p.A., 00131 Roma, Italy. (e-mail: danilor78@gmail.com).

Digital Object Identifier 10.1109/LSP.2014.2301763

vector of the noisy returns representing the lth range cell is given by. $\boldsymbol{z}_l = \boldsymbol{s}_l + \boldsymbol{n}_l \in \mathbb{C}^{N\times 1}$, where $\boldsymbol{s}_l = \alpha\chi_p(-\epsilon_0, f)\boldsymbol{v}$ if $l = l_0$; $\boldsymbol{s}_l = \alpha\chi_p(T_p - \epsilon_0, f)\boldsymbol{v}$ if $l = l_0 + 1$; $\boldsymbol{s}_l = 0$ if $l \neq l_0, l_0 + 1$. In the previous equations, l_0 is the cell under test, $\boldsymbol{v}$ is the overall space-time steering vector[1] [10], [15]; $\chi_p(\cdot,\cdot)$ is the complex ambiguity function of the transmitted pulse waveform [15], 0 is the null vector of proper dimensions, and ϵ_0 is a residual delay that leads to target energy spillover. The interested reader is referred to [9] for further details on the signal model. An alternative definition of the residual delay accounts for target positions surrounding the considered bin center, namely

$$\epsilon = \begin{cases} \epsilon_0, & \text{if } l = l_0 \text{ and } 0 \le \epsilon_0 \le T_p/2, \\ \epsilon_0 - T_p, & \text{if } l = l_0 + 1 \text{ and } T_p/2 \le \epsilon_0 \le T_p. \end{cases} \quad (1)$$

Finally, the decision problem to be solved can be formulated in terms of the following binary hypothesis test:

$$\begin{cases} H_0 : \boldsymbol{z}_i = \boldsymbol{n}_i, i = l-1, l, l+1;\ \boldsymbol{z}_k = \boldsymbol{n}_k,\ k = 1, \ldots, K, \\ H_1 : \begin{cases} \boldsymbol{z}_{l-1} = \boldsymbol{n}_{l-1},\ 0 < \epsilon \le T_p/2, \\ \boldsymbol{z}_{l-1} = \alpha\chi_p\left(-T_p - \epsilon, f\right)\boldsymbol{v} + \boldsymbol{n}_{l-1}, -T_p/2 \le \epsilon \le 0, \\ \boldsymbol{z}_l = \alpha\chi_p\left(-\epsilon, f\right)\boldsymbol{v} + \boldsymbol{n}_l, \\ \boldsymbol{z}_{l+1} = \alpha\chi_p\left(T_p - \epsilon, f\right)\boldsymbol{v} + \boldsymbol{n}_{l+1},\ 0 < \epsilon \le T_p/2, \\ \boldsymbol{z}_{l+1} = \boldsymbol{n}_{l+1},\ -T_p/2 \le \epsilon \le 0, \\ \boldsymbol{z}_k = \boldsymbol{n}_k,\ k = 1, \ldots, K, \end{cases} \end{cases}$$

where α is a deterministic factor accounting for channel and target effects, f is the target Doppler frequency, $\boldsymbol{n}_i$, $i = l-1, l, l+1$, and $\boldsymbol{n}_k, k = 1, \ldots, K \ge N$, are independent complex normal random vectors with zero mean and covariance matrices $E[\boldsymbol{n}_i\boldsymbol{n}_i^\dagger] = \gamma\boldsymbol{M}$ and $E[\boldsymbol{n}_k\boldsymbol{n}_k^\dagger] = \boldsymbol{M}$, where $\gamma > 0$ and $(\cdot)^\dagger$ denotes conjugate transpose.

In the next section we derive an adaptive decision scheme that takes advantage of the possible spillover of target energy.

III. Detector Design

Denote by $\boldsymbol{Z} = [\boldsymbol{Z}_P\ \boldsymbol{Z}_S]$ the overall data matrix, with $\boldsymbol{Z}_P = [\boldsymbol{z}_{l-1}, \boldsymbol{z}_l, \boldsymbol{z}_{l+1}]$ the primary data matrix, $\boldsymbol{Z}_S = [\boldsymbol{z}_1, \ldots, \boldsymbol{z}_K]$ the secondary data matrix. Moreover, let

$$\chi(\epsilon) = \begin{cases} [0, \chi_p(-T_p - \epsilon, f), \chi_p(-\epsilon, f)]^T, -T_p/2 \le \epsilon \le 0, \\ [\chi_p(-\epsilon, f), \chi_p(T_p - \epsilon, f), 0]^T, 0 < \epsilon \le T_p/2, \end{cases} \quad (2)$$

where $(\cdot)^T$ denotes transpose. The GLRT is the following decision rule

$$\frac{\max\limits_{\epsilon,\gamma,\alpha,\boldsymbol{M}} f_1(\boldsymbol{Z}; \boldsymbol{M}, \gamma, \alpha, \epsilon)}{\max\limits_{\gamma,\boldsymbol{M}} f_0(\boldsymbol{Z}; \boldsymbol{M}, \gamma)} \underset{H_0}{\overset{H_1}{\gtrless}} \eta, \quad (3)$$

where η is the threshold value to be set according to the desired Probability of False Alarm (P_{fa}), and $f_i(\cdot;\cdot)$ is the probability density function (pdf) of $\boldsymbol{Z}$ under the H_i hypothesis, $i = 0, 1$. Assumptions of Section II imply that

$$f_1(\boldsymbol{Z}; \boldsymbol{M}, \gamma, \alpha, \epsilon) = \left[\frac{\mathrm{etr}\left\{-\boldsymbol{M}^{-1}\left(\frac{1}{\gamma}\boldsymbol{u}_1\boldsymbol{u}_1^\dagger + \boldsymbol{S}\right)\right\}}{\pi^N\gamma^{\frac{3N}{K+3}}\det(\boldsymbol{M})}\right]^{K+3} \quad (4)$$

[1]For the sake of brevity, we omit the dependence of $\boldsymbol{v}$ on the spatial and the normalized Doppler frequency.

and

$$f_0(\boldsymbol{Z}; \boldsymbol{M}, \gamma) = \left[\frac{\mathrm{etr}\left\{-\boldsymbol{M}^{-1}\left(\frac{1}{\gamma}\boldsymbol{u}_0\boldsymbol{u}_0^\dagger + \boldsymbol{S}\right)\right\}}{\pi^N\gamma^{\frac{3N}{K+3}}\det(\boldsymbol{M})}\right]^{K+3}, \quad (5)$$

where etr stands for $\exp\{\mathrm{tr}(\cdot)\}$ with $\mathrm{tr}(\cdot)$ being the trace of a square matrix, $\boldsymbol{u}_i = \boldsymbol{Z}_P - i\alpha\boldsymbol{v}\,\boldsymbol{\chi}(\epsilon)^T$, $i = 0, 1$, $\boldsymbol{S} = \boldsymbol{Z}_S\boldsymbol{Z}_S^\dagger$ is K times the sample covariance matrix of the secondary data, and $\det(\cdot)$ denotes the determinant of a square matrix.

Let us begin solving the optimization problem under the H_1 hypothesis. It is well known that the maximum likelihood estimate of $\boldsymbol{M}$, $\widehat{\boldsymbol{M}}$ say, is given by the sample covariance matrix [1]. Replacing $\boldsymbol{M}$ with $\widehat{\boldsymbol{M}}$ in (4) yields

$$f_1(\boldsymbol{Z}; \widehat{\boldsymbol{M}}, \alpha, \gamma, \epsilon) \propto \left[\gamma^{\frac{3N}{K+3}}\det\left(\frac{1}{\gamma}\boldsymbol{u}_1\boldsymbol{u}_1^\dagger + \boldsymbol{S}\right)\right]^{-(K+3)}, \quad (6)$$

where $\propto$ denotes proportionality. Now maximization with respect to α is tantamount to minimizing $\det[(1/\gamma)\boldsymbol{u}_1\boldsymbol{u}_1^\dagger + \boldsymbol{S}]$, that can be recast as follows

$$\begin{aligned} &\gamma^{-3}\det[\boldsymbol{S}]\det[\gamma\boldsymbol{I}_3 + \boldsymbol{u}_1^\dagger\,\boldsymbol{S}^{-1}\boldsymbol{u}_1] \\ &= \gamma^{-3}\det[\boldsymbol{S}]\det[\gamma\boldsymbol{I}_3 + \boldsymbol{u}_1^\dagger\,\boldsymbol{S}^{-1/2}(\boldsymbol{P}_{v_s} + \boldsymbol{P}_{v_s}^\perp)\boldsymbol{S}^{-1/2}\boldsymbol{u}_1] \\ &= \gamma^{-3}\det[\boldsymbol{S}]\det[\boldsymbol{A} + \boldsymbol{u}_1^\dagger\,\boldsymbol{S}^{-1/2}\,\boldsymbol{P}_{v_s}\,\boldsymbol{S}^{-1/2}\boldsymbol{u}_1] \\ &= \gamma^{-3}\det[\boldsymbol{S}]\det[\boldsymbol{A}]\left[1 + \frac{\boldsymbol{v}^\dagger\boldsymbol{S}^{-1}\boldsymbol{u}_1\boldsymbol{A}^{-1}\boldsymbol{u}_1^\dagger\,\boldsymbol{S}^{-1}\boldsymbol{v}}{\boldsymbol{v}^\dagger\boldsymbol{S}^{-1}\boldsymbol{v}}\right] \end{aligned} \quad (7)$$

with $\boldsymbol{A} = \gamma\boldsymbol{I}_3 + \boldsymbol{Z}_P^\dagger\boldsymbol{S}^{-1/2}\boldsymbol{P}_{v_s}^\perp\boldsymbol{S}^{-1/2}\boldsymbol{Z}_P$, $\boldsymbol{I}_N$ the N-dimensional identity matrix, $\boldsymbol{P}_{v_s}^\perp = \boldsymbol{I}_N - \boldsymbol{P}_{v_s}$ with $\boldsymbol{P}_{v_s} = \boldsymbol{S}^{-1/2}\boldsymbol{v}\,\boldsymbol{v}^\dagger\boldsymbol{S}^{-1/2}/\boldsymbol{v}^\dagger\boldsymbol{S}^{-1}\boldsymbol{v}$. Setting to zero the derivative with respect to α of the last factor in (7) yields

$$\widehat{\alpha} = \frac{\boldsymbol{v}^\dagger\boldsymbol{S}^{-1}\boldsymbol{Z}_P\boldsymbol{A}^{-1}\,\boldsymbol{\chi}(\epsilon)^*}{\boldsymbol{\chi}(\epsilon)^T\boldsymbol{A}^{-1}\boldsymbol{\chi}(\epsilon)^*\boldsymbol{v}^\dagger\boldsymbol{S}^{-1}\boldsymbol{v}} = \frac{\widehat{\alpha}_N}{\widehat{\alpha}_D}, \quad (8)$$

where $(\cdot)^*$ denotes complex conjugate. It follows that

$$(6) \propto \left[\frac{\left(\gamma^{\frac{3N-3K-9}{K+3}}\det[\boldsymbol{A}]\right)^{-1}}{1 + \frac{\boldsymbol{v}^\dagger\boldsymbol{S}^{-1}\boldsymbol{Z}_P\boldsymbol{A}^{-1}\boldsymbol{Z}_P^\dagger\,\boldsymbol{S}^{-1}\boldsymbol{v}}{\boldsymbol{v}^\dagger\boldsymbol{S}^{-1}\boldsymbol{v}} - \frac{|\widehat{\alpha}_N|^2}{\widehat{\alpha}_D}}\right]^{K+3}. \quad (9)$$

Let us focus on the denominator of the above equation and observe that $\boldsymbol{A}_1 = \boldsymbol{Z}_P^\dagger\boldsymbol{S}^{-1/2}\boldsymbol{P}_{v_s}^\perp\boldsymbol{S}^{-1/2}\boldsymbol{Z}_P = \boldsymbol{U}\,\boldsymbol{\Lambda}\,\boldsymbol{U}^\dagger$, where $\boldsymbol{\Lambda}$ is a diagonal matrix containing the eigenvalues, λ_i, $i = 1, 2, 3$, of $\boldsymbol{A}_1$ and $\boldsymbol{U}$ is a unitary matrix. Thus, the $(K+3)$ th root of the denominator at the right-hand side of (9) can be recast as

$$\gamma^{\frac{3N-3K-9}{K+3}}\prod_{i=1}^{3}(\gamma + \lambda_i)\left[1 + \sum_{i=1}^{3}\frac{b_i}{\gamma + \lambda_i} - \frac{\left|\sum_{i=1}^{3}\frac{e_i}{\gamma+\lambda_i}\right|^2}{\sum_{i=1}^{3}\frac{a_i}{\gamma+\lambda_i}}\right], \quad (10)$$

where $a_i = |\chi_i|^2$, $b_i = |v_i|^2$, and $e_i = v_i^* \chi_i$, $i = 1,2,3$, with $\boldsymbol{U}^\dagger \boldsymbol{\chi}(\epsilon)^* = [\chi_1, \chi_2, \chi_3]^T$ and $\boldsymbol{U}^\dagger \boldsymbol{Z}_P^\dagger \boldsymbol{S}^{-1}\boldsymbol{v}/\sqrt{\boldsymbol{v}^\dagger \boldsymbol{S}^{-1}\boldsymbol{v}} = [v_1, v_2, v_3]^T$. It follows that (10) can be written as

$$\gamma^e \left[\gamma^3 + \sum_{i=0}^{2} \gamma^i h_{3-i} - \left(\sum_{i=0}^{4} \gamma^i k_{5-i} \right) / \left(\sum_{i=0}^{2} \gamma^i d_{3-i} \right) \right], \tag{11}$$

where $e = (3N - 3K - 9)/(K+3)$, $h_1 = \sum_{i=1}^3 \lambda_i + \sum_{i=1}^3 b_i$, $h_2 = \sum_{i=1}^3 \prod_{j\neq i} \lambda_j + \sum_{i=1}^3 b_i \sum_{j\neq i} \lambda_j$, $h_3 = \lambda_1\lambda_2\lambda_3 + \sum_{i=1}^3 b_i \prod_{j\neq i} \lambda_j$, $d_1 = \sum_{i=1}^3 a_i$, $d_2 = \sum_{i=1}^3 a_i \sum_{j\neq i} \lambda_j$, $d_3 = \sum_{i=1}^3 a_i \prod_{j\neq i} \lambda_j$, $k_1 = p_1 + q_1$, $k_2 = p_2 + q_2$, $k_3 = p_3 + q_3$, $k_4 = p_4 + q_4$, $k_5 = p_5 + q_5$. Moreover, $p_1 = \sum_{i=1}^3 |e_i|^2$, $p_2 = \sum_{i=1}^3 |e_i|^2 \sum_{j\neq i} 2\lambda_j$, $p_3 = \sum_{i=1}^3 |e_i|^2 [(\sum_{j\neq i} \lambda_j)^2 + 2\prod_{j\neq i} \lambda_j]$, $p_4 = \sum_{i=1}^3 |e_i|^2 (2\prod_{j\neq i} \lambda_j)(\sum_{j\neq i} \lambda_j)$, $p_5 = \sum_{i=1}^3 |e_i|^2 \prod_{j\neq i} \lambda_j^2$, $q_1 = 2\sum_{i=1}^3 y_i$, $q_2 = 2\sum_{i=1}^3 y_i(\sum_{j\neq i} \lambda_j + 2\lambda_i)$, $q_3 = 2\sum_{i=1}^3 y_i(\prod_{j\neq i} \lambda_j + \lambda_i^2 + \lambda_i \sum_{j\neq i} \lambda_j)$, $q_4 = 2\sum_{i=1}^3 y_i(2\lambda_i \prod_{j\neq i} \lambda_j + \lambda_i^2 \sum_{j\neq i} \lambda_j)$, $q_5 = 2\sum_{i=1}^3 y_i(\lambda_i^2 \prod_{j\neq i} \lambda_j)$, where $y_1 = \mathrm{Re}\{e_1 e_2^*\}$, $y_2 = \mathrm{Re}\{e_1 e_3^*\}$, $y_3 = \mathrm{Re}\{e_2 e_3^*\}$, and $\mathrm{Re}(\cdot)$ denotes the real part of the argument. Finally, (11) can be recast as

$$g(\gamma) = \gamma^e \left(\sum_{i=0}^{5} \gamma^i w_{6-i} \right) / \left(\sum_{i=0}^{2} \gamma^i d_{3-i} \right), \tag{12}$$

where $w_1 = d_1$, $w_2 = h_1 d_1 + d_2 - k_1$, $w_3 = h_2 d_1 + h_1 d_2 + d_3 - k_2$, $w_4 = h_3 d_1 + h_2 d_2 + h_1 d_3 - k_3$, $w_5 = d_2 h_3 + h_2 d_3 - k_4$, $w_6 = h_3 d_3 - k_5$. Now, we prove that (12) as function of γ admits an absolute minimum in the open interval $\Omega = (0, +\infty)$ and the minimum point is such that $g'(\gamma) = 0$ with $g'(\cdot)$ denoting the derivative of g with respect to γ. To this end, we observe that (12) is continuous and differentiable in Ω, $\lim_{\gamma \to 0^+} g(\gamma) = +\infty$ (note[2] that if $K \geq N$, then $e < 0$), and $\lim_{\gamma \to +\infty} g(\gamma) = +\infty$ if $e + 3 > 0$, which implies $N > 0$. Hence, there exists at least a point $\bar{\gamma} \in \Omega$ such that $g'(\bar{\gamma}) = 0$ and the optimal solution of (12) has to be searched among the stationary points. To proceed further, we set to zero the derivative of g with respect to γ of (12), i.e.,

$$\gamma^{-1} \left(\sum_{i=0}^{7} \gamma^i A_{8-i} \right) \left(\sum_{i=0}^{2} \gamma^i d_{3-i} \right)^{-2} = 0, \tag{13}$$

where $A_1 = d_1 w_1 (3+e)$, $A_2 = d_1 w_2 (2+e) + d_2 w_1 (4+e)$, $A_3 = 5 w_1 d_3 + 3 d_2 w_2 + d_1 w_3 + d_1 e w_3 + d_2 e w_2 + d_3 e w_1$, $A_4 = 4 w_2 d_3 + 2 d_2 w_3 + d_1 e w_4 + d_2 e w_3 + d_3 e w_2$, $A_5 = 3 w_3 d_3 + d_2 w_4 - d_1 w_5 + d_1 e w_5 + d_2 e w_4 + d_3 e w_3$, $A_6 = 2 w_4 d_3 - 2 d_1 w_6 + d_1 e w_6 + d_2 e w_5 + d_3 e w_4$, $A_7 = w_5 d_3 - d_2 w_6 + d_2 e w_6 + d_3 e w_5$, $A_8 = d_3 e w_6$, and select the positive root, $\widehat{\gamma}_1$ say, which returns the minimum of g. It is important to observe that since the degree of the numerator of (13) is 7, due to Abel's Impossibility Theorem, the roots of a general 7th order polynomial can only be computed (to any desired degree of accuracy) using numerical algorithms such as the Newton-Raphson or Laguerre methods. Nevertheless, resorting to Rouchè Theorem, it is always possible to provide upper and lower bounds concerning the magnitude of the roots, which can be used for the implementation of the Newton-Raphson procedure. Specifically, the lower and the upper bounds are given by $\gamma_l = \frac{|A_8|}{|A_8| + \max\{|A_1|, \ldots, |A_7|\}}$ and $\gamma_u = 1 + \frac{1}{|A_1|} \max\{|A_2|, \ldots, |A_8|\}$, respectively. On the other hand, under the H_0 hypothesis, the optimization with respect to yields

$$f_0(\boldsymbol{Z}; \widehat{\boldsymbol{M}}, \gamma) \propto \left\{ \gamma^e \prod_{i=1}^{3} (\gamma + \mu_i) \right\}^{-(K+3)}, \tag{14}$$

where μ_i, $i = 1,2,3$, are the eigenvalues of $\boldsymbol{Z}_P^\dagger \boldsymbol{S}^{-1} \boldsymbol{Z}_P$. By Proposition 2 of [13], it is easy to prove that $g(\gamma) = \gamma^e \prod_{i=1}^3 (\gamma + \mu_i)$ admits a unique absolute minimum if $N < K+3$. The minimum point is given by the unique positive root, $\widehat{\gamma}_0$ say, of the equation $\gamma^{e-1}[B_1\gamma^3 + B_2\gamma^2 + B_3\gamma + B_4] = 0$, where $B_1 = e + 3$, $B_2 = (\mu_1 + \mu_2 + \mu_3)(e+2)$, $B_3 = (\mu_1\mu_2 + \mu_1\mu_3 + \mu_2\mu_3)(e+1)$, $B_4 = e\mu_1\mu_2\mu_3$.

Gathering the above results, the GLRT can be recast as

$$\max_{\epsilon \in [-T_p/2, T_p/2]} \frac{\widehat{\gamma}_0^{\frac{3N}{K+3}} \det\left[\frac{1}{\widehat{\gamma}_0} \boldsymbol{Z}_P \boldsymbol{Z}_P^\dagger + \boldsymbol{S} \right]}{\widehat{\gamma}_1^{\frac{3N}{K+3}} \det\left[\frac{1}{\widehat{\gamma}_1} \widehat{\boldsymbol{u}}_1 \widehat{\boldsymbol{u}}_1^\dagger + \boldsymbol{S} \right]} \underset{H_0}{\overset{H_1}{\gtrless}} \eta, \tag{15}$$

where $\widehat{\boldsymbol{u}}_1 = \boldsymbol{Z}_P - \widehat{\alpha} \boldsymbol{v} \boldsymbol{\chi}(\epsilon)^T$. Maximization over ϵ cannot be conducted in closed form. Hence, we resort to a grid-search to maximize with respect to ϵ. Any grid-search-based implementation of this detector will be referred to in the following as the GLRT with Localization Capabilities for PHE (GLRT-LC-PHE). Finally, it is not difficult to show that the GLRT-LC-PHE ensures the CFAR property with respect to the interference covariance matrix [9], [16].

IV. Performance Assessment

In this section, we analyze the performance of the proposed detection algorithm in terms of Probability of Detection (P_d) and Root Mean Square (RMS) error in range. For comparison purposes, we also show the performance of the so-called Modified ACE (M-ACE) derived in [9]. The analysis is conducted both on simulated and real recorded data.

As to simulated data, we exploit standard Monte Carlo counting techniques and evaluate the thresholds necessary to ensure a preassigned value of P_{fa} resorting to $100/P_{fa}$ independent trials. The P_d values and the RMS range errors are estimated over 10^4 and 10^3 independent trials, respectively. The actual position of the target is modeled as (independent from trial to trial and) uniformly distributed[3] in $(t_{min} + (l-1)T_p - T_p/2, t_{min} + (l-1)T_p + T_p/2)$. Moreover, we use a rectangular pulse with $T_p = 0.2$ μs and $f = 0$ Hz. As to the ϵ, it takes on values in $\{\frac{n - N_\epsilon}{2N_\epsilon} T_p\}_{n=0}^{2N_\epsilon}$ with $N_\epsilon = 5$. The SNR is given by $SNR = \frac{|\alpha|^2}{\gamma} \boldsymbol{v}^\dagger \boldsymbol{M}^{-1} \boldsymbol{v}$ with α a deterministic factor, while the disturbance is modeled as an exponentially-correlated complex normal vector with one-lag correlation coefficient ρ, namely the (i,j)th element of the covariance matrix $\boldsymbol{M}$ is given by $\rho^{|i-j|}$, with $\rho = 0.9$. Finally, we set $P_{fa} = 10^{-4}$ and $\gamma = 2$.

The detection performances are analyzed in Figs. 1 and 2. More precisely, in Fig. 1 we plot P_d versus SNR for $N = 16$, and two values of K, while in Fig. 2 we report the RMS error in range versus the SNR for the same values of N and K as in Fig. 1. The curves highlight that for a small number of training

[2]The sign of w_6/d_3 can be easily obtained from (9).

[3]Otherwise stated, the residual delay is a realization of the uniform random variable (rv) that takes on values in $[-T_p/2\ T_p/2]$.

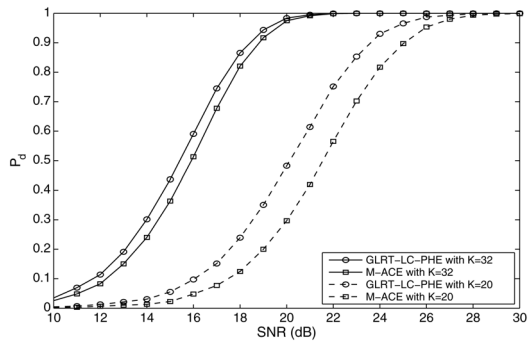

Fig. 1. P_d versus SNR for the GLRT-LC-PHE and the M-ACE with simulated data; $N = 16$ and two values of K.

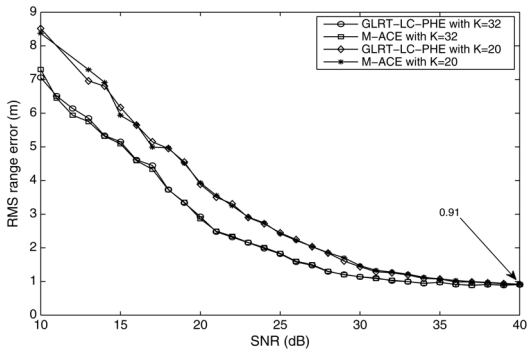

Fig. 2. RMS error in range versus SNR for the GLRT-LC-PHE and the M-ACE with simulated data; $N = 16$ and two values of K.

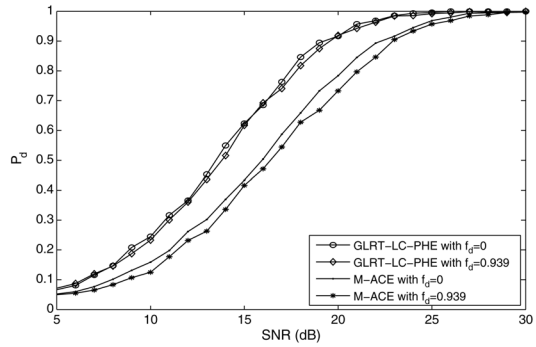

Fig. 3. P_d versus SNR for the GLRT-LC-PHE and the M-ACE with IPIX data; $N = 8$, $K = 10$, $N_\epsilon = 5$, and FA$= 15$.

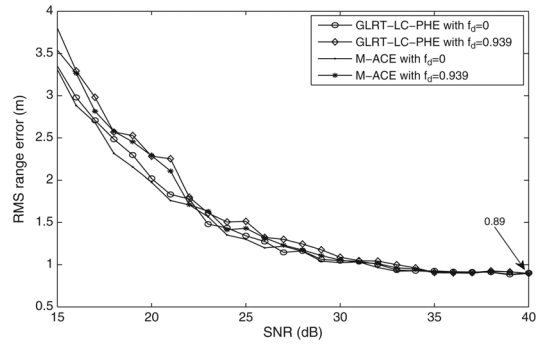

Fig. 4. RMS errors in range versus SNR for the GLRT-LC-PHE and the M-ACE with IPIX data; $N = 8$, $K = 10$, $N_\epsilon = 5$, and FA$= 15$.

data, the GLRT-LC-PHE guarantees a superior detection performance than the M-ACE. For instance, at $P_d = 0.9$, the performance gain is about 1.5 dB when $K = 20$. However, the gain reduces to 0.4 dB when $K = 32$. The curves also show that two detectors share the same performance in terms of target localization capability, which also depends on K. More precisely, the higher K, the lower the RMS error in range. Finally, it is important to observe that for high SNR values the RMS error can be approximated as a rv uniformly distributed in $(-\Delta_r/2, \Delta_r/2)$ with Δ_r denoting the search grid resolution [9]. The standard deviation of such rv (i.e., $\Delta_r/\sqrt{12}$) is a lower-bound on the RMS errors, that for the considered parameter values is equal to 0.866 m (see Figs. 2 and 4).

In Figs. 3 and 4, we study the performance of the GLRT-LC-PHE and the M-ACE using data collected by the McMaster IPIX radar from a site in Dartmouth in November 1993 [17]. Our analysis refer to the file 19931117 131609 stareB0002.cdf (dataset 226 of [17]). The details on the experiment can be found in [17]. We use the range cells 49-51 of VV channel as the primary data, and the range cells adjacent to the primary data as the secondary data; specifically, we choose the range cells 44-48 and 52-56. The normalized Doppler frequency is selected equal to 0 and 0.939 (which corresponds to a moving target with velocity of about 15 m/s).

The P_d and the RMS error in range are evaluated over 1536 and 500 independent trials, respectively. Moreover, we investigate the behaviors of the GLRT-LC-PHE and M-ACE under the same number of False Alarms (FA). The limited amount of real data does not allow a Monte Carlo estimation of the P_{fa} on live clutter. Nevertheless, we set the threshold of the different receivers in order to obtain a pre-assigned FA number, i.e., FA $= 15$. Inspection of the figures confirms the trend observed in Figs. 1 and 2. Specifically, the GLRT-LC-PHE ensures better detection performance than the M-ACE; as to the localization capabilities, both receivers exhibit the same behavior, namely the RMS errors are comparable for the considered SNR values.

V. Conclusions

In this work, we have considered the problem of adaptive detection and range estimation of a point-like target buried in partially homogeneous Gaussian disturbance. At the design stage, we have exploited target energy spillover to derive an adaptive receiver with localization capabilities. Remarkably, it ensures the desirable CFAR property with respect to the unknown parameters of the interference. The performance assessment, conducted on both simulated data and real recorded data, has shown that, for the considered values of the parameters, the new receiver can guarantee better detection performances than the M-ACE [9] at the price of an increased computational load. On the other hand, the estimation accuracy of the target position is comparable to that of the M-ACE. Possible future research tracks might include the design of decision schemes with localization capabilities for range-distributed targets and/or polarization processing [18].

Acknowledgment

The authors thank the Associate Editor, Prof. J. Tabrikian, and the anonymous reviewers for the helpful comments leading to the improvement of the paper.

REFERENCES

[1] E. J. Kelly, "An adaptive detection algorithm," *IEEE Trans. Aerosp. Electron. Syst.*, vol. AES-22, no. 2, pp. 115–127, Mar. 1986.

[2] E. J. Kelly and K. Forsythe, Adaptive Detection and Parameter Estimation for Multidimensional Signal Models Lincoln Lab, Mass. Inst. Technol., Lexington, MA, USA, Tech. Rep. 848, Apr. 19, 1989.

[3] F. C. Robey, D. L. Fuhrman, E. J. Kelly, and R. Nitzberg, "A CFAR adaptive matched filter detector," *IEEE Trans. Aerosp. Electron. Syst.*, vol. 29, no. 1, pp. 208–216, Jan. 1992.

[4] Y. I. Abramovich, N. K. Spencer, and A. Y. Gorokhov, "Modified GLRT and AMF framework for adaptive detectors," *IEEE Trans. Aerosp. Electron. Syst.*, vol. 43, no. 3, pp. 1017–1051, Jul. 2007.

[5] W. L. Melvin, "Space-time adaptive radar performance in heterogeneous clutter," *IEEE Trans. Aerosp. Electron. Syst.*, vol. 36, no. 2, pp. 621–633, Apr. 2000.

[6] S. Kraut and L. L. Scharf, "The CFAR adaptive subspace detector is a scale-invariant GLRT," *IEEE Trans. Signal Process.*, vol. 47, no. 9, pp. 2538–2541, Sep. 1999.

[7] E. Conte, M. Lops, and G. Ricci, "Asymptotically optimum radar detection in compound gaussian noise," *IEEE Trans. Aerosp. Electron. Syst.*, vol. 31, no. 2, pp. 617–625, Apr. 1995.

[8] X. Zhang, P. K. Willett, and Y. Bar-Shalom, "Monopulse radar detection and localization of multiple unresolved targets via joint bin processing," *IEEE Trans. Signal Process.*, vol. 53, no. 4, pp. 1225–1236, Apr. 2005.

[9] D. Orlando and G. Ricci, "Adaptive radar detection and localization of a point-like target," *IEEE Trans. Signal Process.*, vol. 59, no. 9, pp. 4086–4096, Sep. 2011.

[10] J. R. Guerci, *Space-Time Adaptive Processing for Radar*. Norwood, MA, USA: Artech House, 2003.

[11] M. C. Wicks, M. Rangaswamy, R. Adve, and T. D. Hale, "Space-time adaptive processing: A knowledge-based perspective for airborne radar," *IEEE Signal Process. Mag.*, vol. 23, no. 1, pp. 52–65, Jan. 2006.

[12] K. Gerlach and M. J. Steiner, "Adaptive detection of range distributed targets," *IEEE Trans. Signal Process.*, vol. 47, no. 7, pp. 1844–1851, Jul. 1999.

[13] E. Conte, A. De Maio, and G. Ricci, "GLRT-based adaptive detection algorithms for range-spread targets," *IEEE Trans. Signal Process.*, vol. 49, no. 7, pp. 1336–1348, Jul. 2001.

[14] C. Hao, J. Yang, X. Ma, C. Hou, and D. Orlando, "Adaptive detection of distributed targets with orthogonal rejection," *IET Radar, Sonar Navig.*, vol. 6, no. 6, pp. 483–493, Jul. 2012.

[15] F. Bandiera, D. Orlando, and G. Ricci, *Advanced radar detection schemes under mismatched signal models*. San Rafael, CA, USA: Morgan & Claypool, 2009, Synthesis Lectures on Signal Processing No. 8.

[16] E. Conte, A. De Maio, and G. Ricci, "GLRT-Based adaptive detection algorithms for range-spread targets," *IEEE Trans. Signal Process.*, vol. 49, no. 7, pp. 1336–1348, Jul. 2001.

[17] [Online]. Available: http://soma.crl.mcmaster.ca/ipix/

[18] M. Hurtado, S. Gogineni, and A. Nehorai, "Adaptive polarization design for target detection and tracking," in *Waveform Design and Diversity for Advanced Radar Systems*, F. Gini, A. De Maio, and L. Patton, Eds. Stevenage, U.K.: IET, 2011, ch. 16, pp. 453–496.